Measurement System for Attitude of Anterior Pelvic Plane and Implantation of Prothesis in THR Surgery

Hong Chen, *Senior Member, IEEE*, Zhe Cao, Shaojie Su, Jie Liu, and Zhihua Wang, *Fellow, IEEE*

***Abstract*— With the average age of population increasing in the world, the number of total hip replacement (THR) surgeries increases year by year. However, the failure rate of THR surgeries is up to 10% following primary surgery and 28% after revision arthroplasty, which has direct correlation to the implantation angles between prosthesis and pelvis. To improve the implanting accuracy of the prosthesis, we propose a measurement system and estimation algorithms. The system includes three parts: an initial attitude measurement instrument, which is used to determine the initial attitude of the anterior pelvic plane (APP), a real-time attitude measurement instrument, which aims to acquire the real-time attitude of the APP, and an acetabular cup angle measurement instrument, which obtains the relative angles between prosthesis and pelvis. Each of them is based on inertial measurement unit (IMU) and magnetometer. A quaternion-based extended Kalman filter is adopted to fuse the data from IMU and magnetometer to estimate the orientation, and the algorithm calculating the attitude of pelvis and relative angles between pelvis and prosthesis is designed in this paper. The reliability of this system, from the measurement point of view, has been verified by experiments. The experimental results show that the root-mean-square errors of APP attitude and acetabular cup implanting orientation are less than 1.6° and 3° with standard uncertainty of less than 0.22° and 0.17°, respectively. The accuracy of our system meets the requirement of the THR surgeries.**

***Index Terms*— Anterior pelvic plane (APP), extended Kalman filter (EKF), inertial measurement unit (IMU), total hip replacement (THR) surgery.**

I. Introduction

With the aging of the population, the number of patients, suffering from hip joint diseases, has a trend of increasing year by year. Total hip replacement (THR) surgery is an orthopedic surgery which replaces the damaged hip joint with prosthesis. In the United States, the demand for THR surgeries is estimated to grow by 174%–572% from 2005 to 2030 [1]. However, there is a failure rate 8%–9% of THR surgeries [2], which would lead to many complications to patients. The complications after THR, such as heterotopic bone formation, mechanical aseptic loosening, superficial and deep infections, prosthetic or periprosthetic fracture, and dislocation [3]–[5], may bring great pain to patients. The most frequent complication is dislocation [6]–[9], which has been reported to be between 0.3% and 10% following primary THR surgeries and up to 28% after revision arthroplasty [9]–[13]. Moreover, the first surgery accounts for the majority of the failures of THR surgeries [13].

Manuscript received October 16, 2017; revised December 31, 2017; accepted February 5, 2018. Date of publication March 14, 2018; date of current version July 12, 2018. This work was supported in part by the National Natural Science Foundation of China under Grant 61674090, in part by the National High Technology Research and Development Program of China (863 Program) under Grant 2015AA016601, and in part by the Beijing Engineering Research Center under Grant BG0149. *(Corresponding author: Hong Chen.)*

The authors are with the Tsinghua National Laboratory for Information Science and Technology, Institute of Microelectronics, Tsinghua University, Beijing 100084, China (e-mail: hongchen@tsinghua.edu.cn).

Color versions of one or more of the figures in this paper are available online at http://ieeexplore.ieee.org.

Digital Object Identifier 10.1109/TIM.2018.2809818

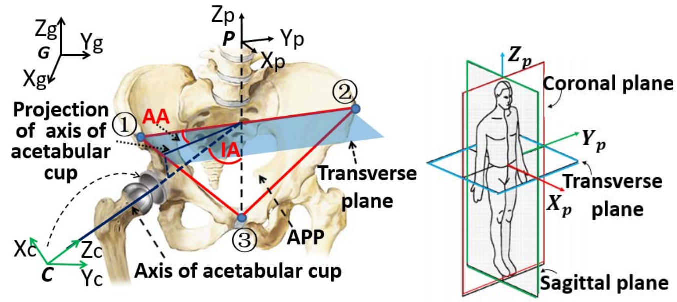

(a) (b)

Fig. 1. Pelvic structure and planes of human body. (a) Definition of APP, AA, and IA. (b) Planes of human body.

The primary cause of dislocation is malposition of acetabular prosthesis [9], [14], [15]. To avoid dislocation, the acetabular prosthesis should be implanted accurately. The optimal ranges for acetabular cup implantation angles had been discussed in [16]–[18]. Lewinnek *et al.* [16] describe a safe zone of 5° –25° for anteversion angle (AA) and 30° –50° for inclination angle (IA), which is widely recognized in medical community. They found that the dislocation rate will decrease four times when placing acetabular cup within this range. In [9], three different kinds of definitions for positioning angles are discussed, that is, operative definition, radiographic definition, and anatomical definition. In this paper, anatomical definition is chosen to establish the positioning angles, in which, AA is the angle between the projection of acetabular cup axis on transverse plane and the y-axis of pelvis, and IA is the angle between the acetabular cup axis and z-axis of pelvis, respectively, as depicted in Fig. 1.

In order to determine the implantation angles, anterior pelvic plane (APP) can be used as a reference plane [19], [22]. The APP is defined by the right and left anterior-superior iliac spine (ASIS) [points, respectively, in Fig. 1(a)] and the pubic tubercle [point ③ in Fig. 1(a)], which is parallel to the coronal plane of human [shown in Fig. 1(b)]. To estimate the attitude of APP, we first define the coordinate frame. In Fig. 1(a), the reference coordinate frame is geodetic (***G***), which is corresponds to south-east-up of the earth, and the coordinate frame of pelvis ($\boldsymbol{P}$) is the same as that of the human body. In other words, X_p is vertical to the APP, Y_p pointed horizontally from left to right, and Z_p vertically upward. In our work, only the axis of the prosthesis cup is needed. Once we align Z_c to the axis, we could define the coordinate frame of prosthesis cup ($\boldsymbol{C}$).

Many efforts have been made to determine the attitude of APP and implantation angles of prosthesis. Widmer [23] discuss and indicate a proper placement for prostheses. Goniometer used to be a traditional device to determine the positioning angles of prosthesis [24], while in practical uses, it has been replaced by visual estimation [25], which is more convenient. Usually, surgeons used to apply preoperative systems to help make plans by reconstructing 3-D models from computed tomography (CT) images [26]. However, during surgeries, preoperative plans often need to be changed and unexpected conditions may occur consequently. Moreover, multidetector-row CT images are adopted to define pelvic anatomical coordinate in [27]. The CT scans and computerized component guidance are widely used to avoid dislocation in THR [28]. However, CT-based system is expensive and increases the operation time; moreover, radiation exposure has great damage to patients. In addition, many intraoperative techniques recommend the floor of the operating room as a reference to place acetabular prosthesis [12], which is mainly depend on the experience of surgeons, leading to more uncertainty.

With the miniaturization and practicality of inertial measurement unit (IMU), researchers have tried to use them to measurement joint angles. Favre *et al.* [29] measure 3-D knee joint angle outside a laboratory for clinical examination and therapeutic treatment comparison. Šlajpah *et al.* [30] apply inertial sensors to assess the motion in human walking. Zhang *et al.* [31] reveal the accuracy of an IMU system for estimating rotations across the hip, knee, and ankle during level walking, stair ascent, and stair descent. In [32], IMU is used for robust estimation of position and orientation of a freely moving target in surgical applications. Sabatelli *et al*. [33] adopt 9-D IMU in an application-specific integrated processor for an angular estimation system. Moreover, a method is proposed to estimate the transducer attitudes using only their own measurements without depending on reference motion data. Without a gyroscope, the IMU employs solely accelerometers to capture the motion of a body in the form of its linear and angular acceleration as well as its angular velocity in [34]. However, few people use these sensors for attitude estimation of APP in THR surgery. In [35], a measurement instrument based on IMU and magnetometers has been used to estimate the initial attitude of the APP. In this paper, we design an IMU-based system to estimate the attitude of APP and implantation angles of prosthesis in THR. The system is comprised of three parts: inertial attitude measurement instrument (IAMI), real-time attitude measurement instrument (RAMI), and acetabular cup angle measurement instrument (AAMI). Each of them is based on IMU and magnetometer. The measurement system deals with four things.

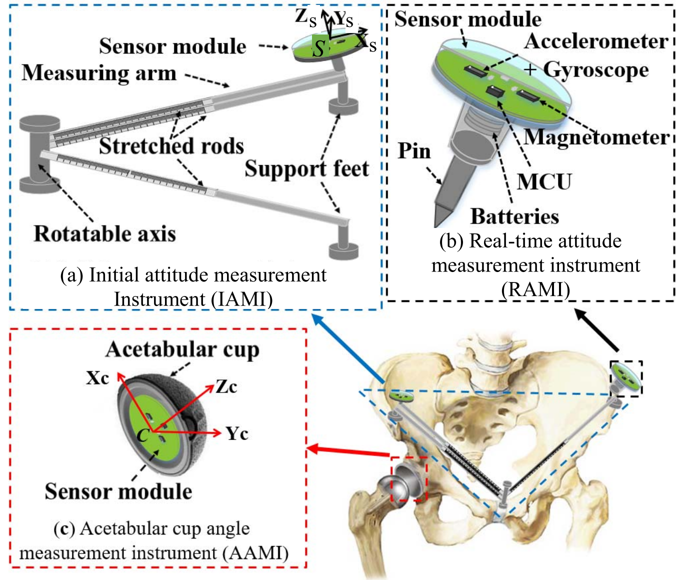

Fig. 2. Architecture of the measurement system. (a) Initial attitude measurement instrument. (b) Real-time attitude measurement instrument. (c) Acetabular cup angle measurement instrument.

1) Acquire the attitude of the measurement device itself by fusing sensor data obtained from IMU and magnetometer sensors.
2) Calculate the initial attitude of APP with IAMI.
3) Obtain the transformation relation between the initial attitude of APP and the RAMI, which is fixed on pelvis, and measure the real-time attitude of the APP.
4) Acquire the implantation angles between the cup axis and the APP by attaching AAMI to acetabular cup.

The algorithms for 2)– 4) are designed in this paper. The main contribution of this paper is to provide a novel system including instruments and algorithms to measure the APP during the surgery. With the help of the system, surgeon could make an accurate judgment of the implanting position of the acetabular cup during the surgery instead of the estimate it just by their experience. As a result, the success rate of the THR surgery could be improved.

The rest of this paper is organized as follows. In Section II, the architecture of the measurement system is represented. The estimation algorithms designed for attitude measurement of APP and implantation angles for prosthesis are discussed in Section III. In Section IV, the experimental results are described. Finally, the conclusion is drawn in Section V.

II. System Architecture

The architecture of the proposed measurement system (shown in Fig. 2) is composed of three parts: the first one [shown in Fig. 2(a)] is IAMI, which is used to acquire the initial attitude of the APP, the second part [shown in Fig. 2(b)] is RAMI, which tracks the real-time motion of the APP during THR, and the third part [shown in Fig. 2(c)] is AAMI, which is comprised of a prosthesis cup and a sensor module, used for measurement of implantation angles of acetabular cup. IAMI consists of a sensor module, a rotatable axis, three support feet, a measuring arm, and two stretched rods. The measuring arm could rotate around the rotatable axis from one stretched rod to another. We design the support feet to avoid the inclination of the sensor module. During the THR surgery, this device would be placed on the APP to obtain the initial attitude of the pelvis. RAMI, which would be fixed on one of the ASISs, is comprised of a sensor module and a connecting pin. The AAMI consists a sensor module which could be attached to acetabular cup. Each part has the same sensor modules, which are comprised of a microcontroller unit, an IMU, and a magnetometer sensor.

In order to acquire the precise attitude of the APP, we define the coordinate of sensor module, which is called navigation coordinate frame (S), in which, Z_s is perpendicular to the sensor module board, while X_s and Y_s are align with the sensors on the board. We adjust the axis X_s of the sensor module on IAMI parallel to the stretched rod, the axis Z_s vertical to the bottom of the sensor module, and the axis Y_s perpendicular to X_s and Z_s. Except for the sensor module, the other parts of IAMI could be manufactured and calibrated as accurate as possible mechanically (such as ± 0.1 mm machining accuracy or better). As the IMU-based sensor module is fixed on the printed circuit board, its body frame of x-, y-, and z-axes could be determined and described clearly in the handbook. That is, it is practicable to align the X_s parallel to the stretched rod mechanically. Similarly, for RAMI, we adjust the axis Z_s of the sensor module aligned with the pin, and for AAMI, the axis Z_s of the sensor module should be parallel to the cup axis Z_c [shown in Fig. 2(c)]. Mechanical calibration is adopted to guarantee the mechanical accuracy. In anatomical definition, the implantation angles are obtained by calculating the relative angles between cup axis Z_c and the axes of APP.

III. Estimation Algorithms for Attitude Measurement of APP and Positioning Angles of Prosthesis

In this paper, a quaternion-based extended Kalman filter (EKF) [32], [33], [36] is adopted to acquire the attitude of the measurement devices, based on the complementary property of IMU and magnetometers [37]. Besides, for calculation of the initial attitude, real-time attitude of APP, and implantation angles of prosthesis, we designed the algorithms, which are discussed as follows.

A. Quaternion-Based EKF for Attitude Estimation

In order to measure the attitude of APP, we first obtain the sensor data collected from IMU and magnetometers. IMU is comprised of a three-axis accelerometer and a three-axis gyroscope. Data collected from accelerometer represents the gravity of three axes of the sensor module that is, $\boldsymbol{a} = [a_x, a_y, a_z]$. Meanwhile, the gyroscope measures three-axis angular velocities of the sensor module, noted as $\boldsymbol{\omega} = [\omega_x, \omega_y, \omega_z]$. Similarly, the data from three-axis magnetometer represent the magnetic force on the sensor module, that is, $\boldsymbol{m} = [m_x, m_y, m_z]$. As we know, accelerometers and magnetometers could measure absolute orientation based on different characteristics of them, but show poor performance in dynamic responses. On the contrary, the gyroscopes have better performance in dynamic responses, but are not good at measuring absolute orientation [38]. Based on the complementary property of IMU and magnetometers, a quaternion-based EKF is adopted for attitude estimation. The state vector $\vec{\boldsymbol{x}}_{\boldsymbol{k}}$ is comprised of rotation quaternion $\vec{\boldsymbol{q}}_{\boldsymbol{k}}$ and gyroscope bias vector ${}^{g}\vec{\boldsymbol{b}}_{\boldsymbol{k}}$, which can be expressed as

$$\vec{\boldsymbol{x}}_{\boldsymbol{k}} = \begin{bmatrix} \vec{\boldsymbol{q}}_{\boldsymbol{k}} \\ {}^{g}\vec{\boldsymbol{b}}_{\boldsymbol{k}} \end{bmatrix} = f\left(\vec{\boldsymbol{x}}_{\boldsymbol{k-1}}\right) + \begin{bmatrix} {}^{q}\vec{\boldsymbol{w}}_{\boldsymbol{k}} \\ {}^{g}\vec{\boldsymbol{w}}_{\boldsymbol{k}} \end{bmatrix} \tag{1}$$

where f is a nonlinear state transition equation at time $\boldsymbol{k}$, ${}^{q}\vec{\boldsymbol{w}}_{\boldsymbol{k}}$ and ${}^{g}\vec{\boldsymbol{w}}_{\boldsymbol{k}}$ are noise vectors of quaternion and gyroscope, respectively. The rotation quaternion $\vec{\boldsymbol{q}}_{\boldsymbol{k}} = [q_0, q_1, q_2, q_3]_k^T$. The nonlinear state transition equation f in (1) can be expressed as

$$f\left(\vec{\boldsymbol{x}}_{\boldsymbol{k-1}}\right) = \begin{bmatrix} I + \frac{1}{2}\boldsymbol{\Omega}_{k-1}(\hat{\boldsymbol{\omega}}) \cdot \nabla T & 0 \\ 0 & I \end{bmatrix} \begin{bmatrix} \vec{\boldsymbol{q}}_{\boldsymbol{k-1}} \\ {}^{g}\vec{\boldsymbol{b}}_{\boldsymbol{k-1}} \end{bmatrix} \tag{2}$$

where $\boldsymbol{\Omega}_{k-1}(\hat{\omega})$ is a matrix for calculating the differential of $\vec{\boldsymbol{q}}_{\boldsymbol{k-1}}$, as shown in the following equation:

$$\begin{aligned} \frac{d}{dt}\vec{\boldsymbol{q}}_{\boldsymbol{k-1}} &= \frac{1}{2}\boldsymbol{\Omega}_{k-1}\left(\hat{\omega}\right)\vec{\boldsymbol{q}}_{\boldsymbol{k-1}} \\ &= \frac{1}{2}\begin{bmatrix} 0 & -\hat{\omega}_x & -\hat{\omega}_y & -\hat{\omega}_z \\ \hat{\omega}_x & 0 & \hat{\omega}_z & -\hat{\omega}_y \\ \hat{\omega}_y & -\hat{\omega}_z & 0 & \hat{\omega}_x \\ \hat{\omega}_z & \hat{\omega}_y & -\hat{\omega}_x & 0 \end{bmatrix}\vec{\boldsymbol{q}}_{\boldsymbol{k-1}} \end{aligned} \tag{3}$$

in which $(\hat{\omega}_x\ \hat{\omega}_y\ \hat{\omega}_z)^T = (\omega_x\ \omega_y\ \omega_z)^T - {}^{g}\vec{\boldsymbol{b}}_{\boldsymbol{k-1}}$ represents the calibrated values of the angular velocity.

The measurement vector $\vec{z}_{\boldsymbol{k}}$ is constructed by staking the accelerometer measurement vector $\vec{\boldsymbol{a}}_{\boldsymbol{k}}$ and the magnetometer measurement vector $\vec{\boldsymbol{m}}_{\boldsymbol{k}}$, as shown in the following equation:

$$\vec{z}_{\boldsymbol{k}} = \begin{bmatrix} \vec{\boldsymbol{a}}_{\boldsymbol{k}} \\ \vec{\boldsymbol{m}}_{\boldsymbol{k}} \end{bmatrix} = \begin{bmatrix} C_g^s(\overrightarrow{\boldsymbol{q}_{\boldsymbol{k}}}) & 0 \\ 0 & C_g^s(\overrightarrow{\boldsymbol{q}_{\boldsymbol{k}}}) \end{bmatrix} \begin{bmatrix} \vec{\boldsymbol{g}} \\ \vec{\boldsymbol{h}} \end{bmatrix} + \begin{bmatrix} {}^{a}\vec{\boldsymbol{v}}_{\boldsymbol{k}} \\ {}^{m}\vec{\boldsymbol{v}}_{\boldsymbol{k}} \end{bmatrix} \tag{4}$$

where $\vec{\boldsymbol{g}}$ and $\vec{\boldsymbol{h}}$ are earth gravity vector and earth magnetism vector in geodetic coordinate frame, and ${}^{a}\vec{\boldsymbol{v}}_{\boldsymbol{k}}$ and ${}^{m}\vec{\boldsymbol{v}}_{\boldsymbol{k}}$ are the noise vectors of the accelerometer and the magnetometer, respectively. In (4), $C_g^s(\vec{\boldsymbol{q}})$ is the transformation matrix to transform $\vec{\boldsymbol{g}}$ and $\vec{\boldsymbol{h}}$ from geodetic coordinate frame to sensor module coordinate frame, as shown in the following equation:

$$\begin{aligned} &C_g^s[\vec{\boldsymbol{q}}] \\ &= \begin{bmatrix} q_0^2+q_1^2-q_2^2-q_3^2 & 2(q_1q_2+q_0q_3) & 2(q_1q_3-q_0q_2) \\ 2(q_1q_2-q_0q_3) & q_0^2-q_1^2+q_2^2-q_3^2 & 2(q_2q_3+q_0q_1) \\ 2(q_1q_3+q_0q_2) & 2(q_2q_3-q_0q_1) & q_0^2-q_1^2-q_2^2-q_3^2 \end{bmatrix}. \end{aligned} \tag{5}$$

Based on the definition of $\vec{\boldsymbol{x}}_{\boldsymbol{k}}$ and $\vec{z}_{\boldsymbol{k}}$ above, EKF algorithm estimates the state vector iteratively, and the specific processing steps are as follows.

1) Acquire current state $\vec{\boldsymbol{x}}_{\boldsymbol{k}}$ based on previous state $\vec{\boldsymbol{x}}_{\boldsymbol{k-1}}$.
2) Calculate the Jacobian matrix $\boldsymbol{F}_{\boldsymbol{k}}$ of $\vec{\boldsymbol{x}}_{\boldsymbol{k}}$ to linearize the system

$$
\begin{aligned}
\boldsymbol{F_k} &= \nabla f_k|_{\vec{x}_k} = \frac{\partial f\,(\vec{\boldsymbol{x}}_{\boldsymbol{k}})}{\partial \vec{\boldsymbol{x}}_{\boldsymbol{k}}} \\
&= \begin{bmatrix}
1 & -T\hat{\omega}_x/2 & -T\hat{\omega}_y/2 & -T\hat{\omega}_z/2 & Tq_1/2 & Tq_2/2 & Tq_3/2 \\
T\hat{\omega}_x/2 & 1 & T\hat{\omega}_z/2 & -T\hat{\omega}_y/2 & -Tq_0/2 & Tq_3/2 & -Tq_2/2 \\
T\hat{\omega}_y/2 & -T\hat{\omega}_z/2 & 1 & T\hat{\omega}_x/2 & -Tq_3/2 & -Tq_0/2 & Tq_1/2 \\
T\hat{\omega}_z/2 & T\hat{\omega}_y/2 & -T\hat{\omega}_x/2 & 1 & Tq_2/2 & -Tq_1/2 & -Tq_0/2 \\
0 & 0 & 0 & 0 & 1 & 0 & 0 \\
0 & 0 & 0 & 0 & 0 & 1 & 0 \\
0 & 0 & 0 & 0 & 0 & 0 & 1
\end{bmatrix}
\end{aligned} \tag{6}
$$

in which $(\hat{\omega}_x\ \hat{\omega}_y\ \hat{\omega}_z)^T = (\omega_x\ \omega_y\ \omega_z)^T - (b_{\omega x}\ b_{\omega y}\ b_{\omega z})^T$, $\hat{\omega}_x, \hat{\omega}_y$, and $\hat{\omega}_z$ represent the calibrated values, and ω_x, ω_y, and ω_z are the measured values.

3) Compute $\vec{\boldsymbol{x}}_{\boldsymbol{k|k-1}}$ and $\boldsymbol{P_{k|k-1}}$ in (7) and (8) with the rediction step of Kalman filter

$$\vec{\boldsymbol{x}}_{\boldsymbol{k|k-1}} = f(\vec{\boldsymbol{x}}_{\boldsymbol{k-1}}, \vec{\boldsymbol{u}}_{\boldsymbol{k-1}}) \tag{7}$$

$$\boldsymbol{P_{k|k-1}} = \boldsymbol{F_{k-1}P_{k-1}F_{k-1}} + \boldsymbol{Q_{k-1}} \tag{8}$$

where $\boldsymbol{P_{k-1}}$ is the covariance of $\vec{\boldsymbol{x}}_{\boldsymbol{k-1}}$, $\boldsymbol{Q_{k-1}}$ is process noise covariance matrix, and $\boldsymbol{P_{k|k-1}}$ is the estimate of the covariance of $\vec{\boldsymbol{x}}_{\boldsymbol{k}}$.

4) Linearize the observation dynamics $\vec{\boldsymbol{z}}_{\boldsymbol{k}} = h\,(\vec{\boldsymbol{x}}_{\boldsymbol{k}}) + \vec{\boldsymbol{v}}_{\boldsymbol{k}}$ as follows:

$$\boldsymbol{H_k} = \nabla h_k|_{\vec{x}_{k|k-1}} = \frac{\partial h(\vec{\boldsymbol{x}}_{\boldsymbol{k}})}{\partial \vec{\boldsymbol{x}}_{\boldsymbol{k}}}. \tag{9}$$

5) Calculate $\vec{\boldsymbol{x}}_{\boldsymbol{k}}$ and $\boldsymbol{P_k}$ in (10) and (11) with the filtering cycle of Kalman filter

$$\vec{\boldsymbol{x}}_{\boldsymbol{k}} = \vec{\boldsymbol{x}}_{\boldsymbol{k|k-1}} + K_k[\vec{\boldsymbol{z}}_{\boldsymbol{k}} - h(\vec{\boldsymbol{x}}_{\boldsymbol{k|k-1}})] \tag{10}$$

$$\boldsymbol{P_k} = [\boldsymbol{I} - \boldsymbol{K_k H_k}]\boldsymbol{P_{k|k-1}} \tag{11}$$

$$\boldsymbol{K_k} = \frac{\boldsymbol{P_{k|k-1}} \cdot \boldsymbol{H_k^T}}{\boldsymbol{H_k} \cdot \boldsymbol{P_{k|k-1}} \cdot \boldsymbol{H_k^T} + \boldsymbol{R_k}} \tag{12}$$

where $\boldsymbol{R_k}$ is the noise covariance of the measurement model and $\boldsymbol{K_k}$ is Kalman gain for iteration k.

B. Estimation of Initial Attitude of APP

In order to obtain the real-time attitude of the APP, we calculate the initial attitude of it. In this paper, we acquire the initial attitude of the APP by calculating the axes vector value of the APP in the reference coordinate frame, that is, geodetic coordinate frame. For measurement of the axes vector of the APP in geodetic coordinate system, we first place the device IAMI on APP (shown in Fig. 3), the rotatable axis is placed on point ③, and the foot of two support arms is placed on points ① and ②, respectively.

To measure the x-axis of APP in geodetic coordinate frame, that is $\vec{\boldsymbol{X}}_{\boldsymbol{p}}^{\boldsymbol{g}}$, we first place the measuring arm of IAMI on lines ①–③ to obtain the vector $\vec{\boldsymbol{x}}_{\boldsymbol{1}}$ in geodetic coordinate frame [shown in (13)]. Next, we rotate the measuring arm around the rotatable axis to line ② and ③ to acquire the vector $\vec{\boldsymbol{x}}_{\boldsymbol{2}}$, as depicted in (14). Then, $\vec{\boldsymbol{X}}_{\boldsymbol{p}}^{\boldsymbol{g}}$, namely, the cross-product of $\vec{\boldsymbol{x}}_{\boldsymbol{1}}$

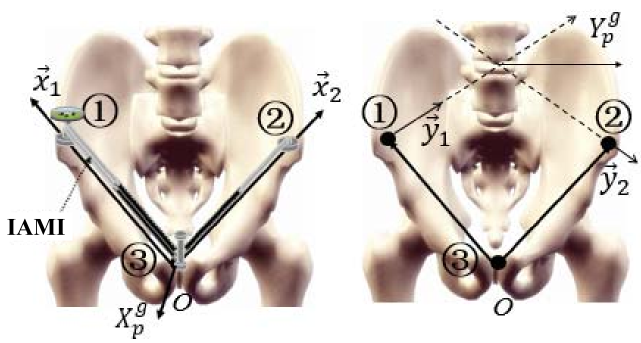

(a) (b)

Fig. 3. Measurement of vector $\vec{\boldsymbol{X}}_{\boldsymbol{p}}^{\boldsymbol{g}}$ and $\vec{\boldsymbol{Y}}_{\boldsymbol{p}}^{\boldsymbol{g}}$ of APP. (a) Measurement of the x-axis vector $\vec{\boldsymbol{X}}_{\boldsymbol{p}}^{\boldsymbol{g}}$. (b) Measurement of the y-axis vector $\vec{\boldsymbol{Y}}_{\boldsymbol{p}}^{\boldsymbol{g}}$.

and $\vec{\boldsymbol{x}}_{\boldsymbol{2}}$, could be calculated in (16)

$$\vec{\boldsymbol{x}}_{\boldsymbol{1}} = \text{angle2dcm (euler1)} \cdot (\vec{\boldsymbol{x}}_{\boldsymbol{0}}) \tag{13}$$

$$\vec{\boldsymbol{x}}_{\boldsymbol{2}} = \text{angle2dcm (euler2)} \cdot (\vec{\boldsymbol{x}}_{\boldsymbol{0}}) \tag{14}$$

$$\vec{\boldsymbol{x}}_{\boldsymbol{0}} = (1, 0, 0)^T \tag{15}$$

$$\vec{\boldsymbol{X}}_{\boldsymbol{p}}^{\boldsymbol{g}} = \vec{\boldsymbol{x}}_{\boldsymbol{2}} \times \vec{\boldsymbol{x}}_{\boldsymbol{1}} \tag{16}$$

where angle2dcm is the transformation function from Euler angle to direction cosine matrix, $\vec{\boldsymbol{x}}_0$ is the unit vector in geodetic coordinate frame.

For the measurement of $\vec{\boldsymbol{Y}}_{\boldsymbol{p}}^{\boldsymbol{g}}$, we first acquire vector $\vec{\boldsymbol{y}}_{\boldsymbol{1}}$ and $\vec{\boldsymbol{y}}_{\boldsymbol{2}}$ in geodetic coordinate frame [shown in Fig. 3(b)], according to (17) and (18). Then, $\vec{\boldsymbol{Y}}_{\boldsymbol{p}}^{\boldsymbol{g}}$ could be calculated based on hypothesis that the pelvis is symmetry, as in (20)

$$\vec{\boldsymbol{y}}_{\boldsymbol{1}} = \text{angle2dcm (euler1)} \cdot (\vec{\boldsymbol{y}}_{\boldsymbol{0}}) \tag{17}$$

$$\vec{\boldsymbol{y}}_{\boldsymbol{2}} = \text{angle2dcm (euler2)} \cdot (\vec{\boldsymbol{y}}_{\boldsymbol{0}}) \tag{18}$$

$$\vec{\boldsymbol{y}}_0 = (0, 1, 0)^T \tag{19}$$

$$\vec{\boldsymbol{Y}}_{\boldsymbol{p}}^{\boldsymbol{g}} = \frac{\vec{\boldsymbol{y}}_{\boldsymbol{1}} + \vec{\boldsymbol{y}}_{\boldsymbol{2}}}{2}. \tag{20}$$

Once $\vec{\boldsymbol{X}}_{\boldsymbol{p}}^{\boldsymbol{g}}$ and $\vec{\boldsymbol{Y}}_{\boldsymbol{p}}^{\boldsymbol{g}}$ have been identified, $\vec{\boldsymbol{Z}}_{\boldsymbol{p}}^{\boldsymbol{g}}$ could also be obtained

$$\vec{\boldsymbol{Z}}_{\boldsymbol{p}}^{\boldsymbol{g}} = \vec{\boldsymbol{X}}_{\boldsymbol{p}}^{\boldsymbol{g}} \times \vec{\boldsymbol{Y}}_{\boldsymbol{p}}^{\boldsymbol{g}}. \tag{21}$$

$\vec{\boldsymbol{X}}_{\boldsymbol{p}}^{\boldsymbol{g}}$ could also been calculated as in (22). Once the vector value of the pelvic axes has been calculated, the attitude (defined as

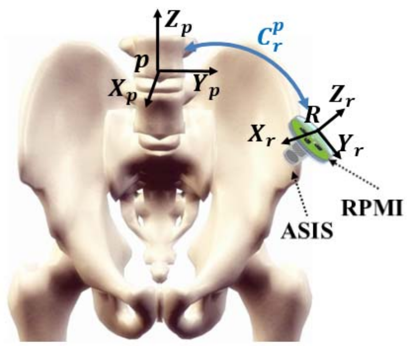

Fig. 4. Relationship between the attitude of RAMI and real-time attitude of APP.

Euler angle) of the APP could be determined, as in (23)

$$\vec{X}_p^g = \begin{bmatrix} c\theta_y c\theta_z & -c\theta_x s\theta_z + s\theta_x s\theta_y c\theta_z & s\theta_x s\theta_z + c\theta_x s\theta_y c\theta_z \\ c\theta_y s\theta_z & c\theta_x c\theta_z + s\theta_x s\theta_y s\theta_z & -s\theta_x c\theta_z + c\theta_x s\theta_y s\theta_z \\ -s\theta_y & s\theta_x c\theta_y & c\theta_x c\theta_y \end{bmatrix} \cdot \vec{x}_0 \tag{22}$$

$$\theta_y = \arcsin(-X_p^g(3)) \tag{23}$$

where c is the abbreviation for operator cos, and s is the abbreviation for operator sin. The initial attitude (defined in Euler angle) of the APP, $\vec{P}_0 = (\theta_x, \theta_y, \theta_z)_{P0}$, could be determined

$$\begin{bmatrix} \theta_y \\ \theta_x \\ \theta_z \end{bmatrix} = \begin{bmatrix} \arcsin(-X_p^g(3)) \\ \arcsin(-Y_p^g(3)/\cos(\theta_y)) \\ \arcsin(X_p^g(2)/\cos(\theta_y)) \end{bmatrix}. \tag{24}$$

C. Real-Time Attitude Estimation of APP

Before the measurement of initial attitude of APP, we fix the device RAMI on one of the ASIS (shown in Fig. 4). The attitude of the RAMI could be obtained by the quaternion-based EKF algorithm. We acquire the real-time attitude of the APP by finding the transformation relationship between the initial attitude of the APP and the attitude of RAMI, because the relative attitude between the APP and RAMI is fixed.

The initial attitude of the APP, $\vec{P}_0 = (\theta_x, \theta_y, \theta_z)_{P0}$, has been obtained in Section III-B. At the same time, the attitude of the RAMI, $\vec{R}_0 = (\theta_x, \theta_y, \theta_z)_{R0}$, could also be gained, because the device RAMI has already been fixed on one side of APP.

The relationship between the APP and RAMI could be calculated as follows:

$$\text{angle2dcm}(\vec{P}_0) = C_r^p \,\text{angle2dcm}(\vec{R}_0). \tag{25}$$

And the transformation matrix C_r^p could be calculated as follows:

$$C_r^p = \text{angle2dcm}(\vec{P}_0) \cdot (\text{angle2dcm}(\vec{R}_0))'. \tag{26}$$

During THR surgery, the transformation matrix remains unchanged, since the RAMI is fixed on the APP. At any moment t, the attitude of the RAMI $\vec{R}_t = (\theta_x, \theta_y, \theta_z)_{Rt}$ could be acquired directly, while the attitude of the pelvis $\vec{P}_t = (\theta_x, \theta_y, \theta_z)_{Pt}$ can be calculated, as follows:

$$\text{angle2dcm}(\vec{P}_t) = C_r^p \,\text{angle2dcm}(\vec{R}_t). \tag{27}$$

In other words, the real-time attitude of APP $\vec{P}_t$ could be acquired by (27).

D. Measurement of Implantation Angles for Prosthesis

As mentioned above, THR is a surgery to replace the damaged hip joint with prosthesis; the most important step is the implantation of the prosthesis. In this paper, the implantation angles of the prosthesis are based on anatomical definition, mentioned in Section I.

For the measurement of IA (IA, shown in Fig. 1), the geodetic coordinate frame $\boldsymbol{G}$ is used as the reference frame. The z-axis of the pelvis $\vec{Z}^p$ should be first transformed from pelvic coordinate frame to geodetic coordinate frame, as shown in (28). Similarly, the acetabular axis $\vec{Z}^c$ should be transformed from the cup coordinate frame to geodetic coordinate frame, as described in (30)

$$\vec{Z}_p^g = C_p^g \cdot \vec{Z}^p \tag{28}$$

$$\vec{Z}^p = (0, 0, 1)^T \tag{29}$$

$$\vec{Z}_c^g = C_c^g \cdot \vec{Z}^c \tag{30}$$

$$\vec{Z}^c = (0, 0, 1)^T \tag{31}$$

where C_p^g is the transform matrix from pelvic coordinate frame to geodetic coordinate frame, and C_c^g is the transform matrix from cup coordinate frame to geodetic coordinate frame. The IA could be determined in

$$\angle \text{IA} = \angle \vec{Z}_p^g \vec{Z}_c^g = \text{acos}\left(\frac{|\vec{Z}_p^g \cdot \vec{Z}_c^g|}{|\vec{Z}_p^g| \cdot |\vec{Z}_c^g|}\right). \tag{32}$$

Similarly, for the measurement of AA (AA, shown in Fig. 1), the pelvic coordinate frame is used as the reference frame. The y-axis of the pelvis $\vec{Y}^p$ is a unit vector [shown in (33)]. While the acetabular axis $\vec{Z}^c$ should be transformed from the cup coordinate frame to the pelvic coordinate frame, which is described in (34). The projection of the acetabular axis on transverse plane in pelvic coordinate frame could be calculated in (36)

$$\vec{Y}^p = (0, 1, 0)^T \tag{33}$$

$$\vec{Z}_c^P = C_c^P \cdot \vec{Z}^c \tag{34}$$

$$\vec{Z}^c = (0, 0, 1)^T \tag{35}$$

$$\vec{Z}_c^{P'} = (\vec{Z}_c^P(1), \vec{Z}_c^P(2), 0)^T \tag{36}$$

where C_c^p is transform matrix from cup coordinate frame to pelvic coordinate frame. The AA could be

$$\angle \text{AA} = \angle \vec{Z}_c^{P'} \vec{Y}^p = \text{acos}\left(\frac{|\vec{Z}_c^{P'} \cdot \vec{Y}^p|}{|\vec{Z}_c^{P'}| \cdot |\vec{Y}^p|}\right). \tag{37}$$

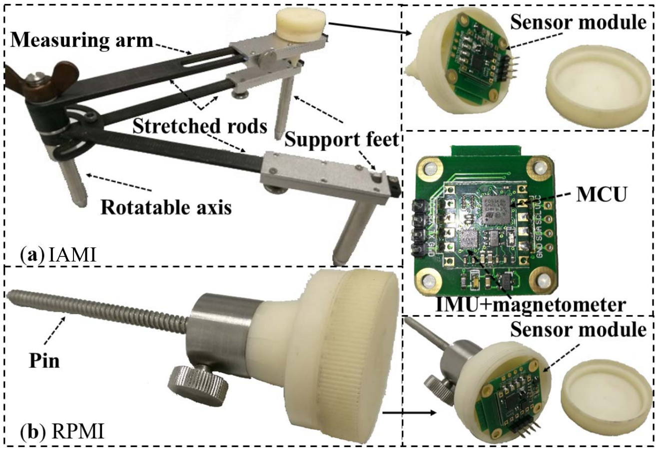

Fig. 5. Proposed system for attitude estimation of APP. (a) IAMI, which is comprised of stretched rods, a rotatable axis, and a sensor module. (b) RAMI, which is comprised of a sensor module and a pin fixed on the bottom of it.

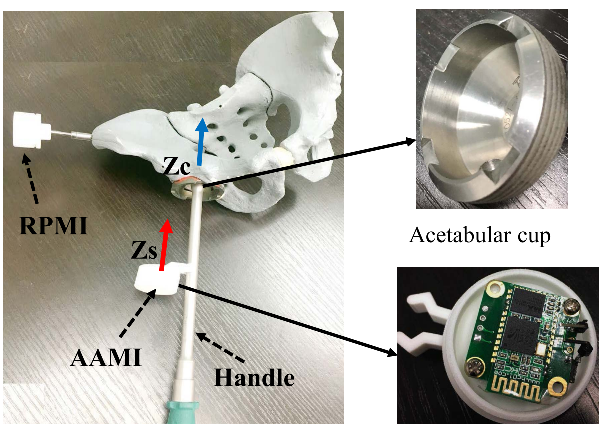

Fig. 6. Customized platform for positioning angles of acetabular cup, the RAMI is fixed on the one side of pelvis, and AAMI is attached to the handle.

IV. Experimental Results and Measurement Uncertainty Discussion

A. Designed Measurement System

The designed measurement system is shown in Fig. 5. The instrument in Fig. 5(a) is IAMI, which is comprised of two stretched rods, a rotatable axis, a measuring arm, and a sensor module. And the instrument in Fig. 5(b) is RAMI, including the same sensor module as that in IAMI and a pin fixed on the bottom of the module. IAMI and RAMI are used to estimate the attitude of APP. AAMI (shown in Fig. 6) is applied to measure the implantation angles of the acetabular cup. In real case, the sensor module of AAMI will not be put into the acetabular cup trial as shown in Fig. 2(c), which will be fixed on a handle. The handle is made of biocompatible material and attached with the acetabular cup. The sensor module is fixed in the box and the box is attached to the handle. As the center line of the handle is designed to be the same as the z-axis, Z_c of the cup, we align the z-axis of the sensor module, denoted by Z_s, parallel to the cup axis Z_c. The data from sensor module are transmitted by Bluetooth.

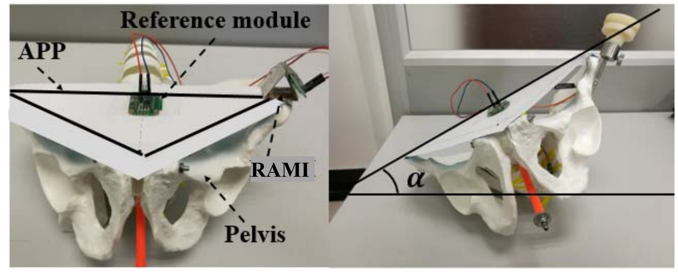

(a) (b)

Fig. 7. Test module and method. (a) Initial attitude of APP. (b) One posture of pelvis in test procedure.

TABLE I
Comparison Between Real Attitude and Estimated Attitude of APP

	Attitude of reference sensor module			Attitude of APP estimated from RAMI		
Euler(°) Axis / State	x-angle	y-angle	z-angle	x-angle	y-angle	z-angle
s1	-26.4	0.13	-2.14	-26.7	0.68	-2.49
s2	-50.8	-0.58	-5.82	-51.1	0.48	-6.26
s3	24.6	1.23	4.21	25.2	0.67	4.58
s4	48.9	0.11	26.6	49.9	-.077	27.9
s5	-2.0	35.7	-48.8	-0.52	36.34	-45.8
s6	-1.80	8.34	-5.04	-1.46	8.46	-3.0

B. Experimental Results of Attitude Estimation of APP

In our previous work, the initial attitude estimation of the APP had been verified in [35]. In order to examine the real-time attitude of APP, we place the pelvis in seven different postures, to obtain different results of the attitude, and Fig. 7(b) shows one posture of the pelvis. In Fig. 7(a), the flat board covered on the pelvis module represents the APP. The real attitude of the APP is acquired from the reference sensor module, which is parallel to the coordinate of APP, while the estimated attitude is resolved from the data, collected by RAMI. By comparing the real and estimated attitude of the APP in different postures, we evaluate the reliability of the measurement system and method proposed in this paper.

In the experiment, the APP had been set at seven different postures s0–s6, the pelvis keeps static at each posture, and the initial attitude is calculated at s0. The three angles including x-, y-, and z-angles represent the angles around x-, y-, and z-axes, respectively. The attitude of APP is acquired from the reference module directly, and with the attitude of the RAMI combined with the initial attitude of APP, the estimated attitude of pelvis could be calculated. The comparison between the real and estimated attitude of pelvis is summarized in Table I. The Euler angle errors of the estimation attitude results of APP compared with the real attitude are shown in Fig. 8. The horizontal axis represents time, and the vertical

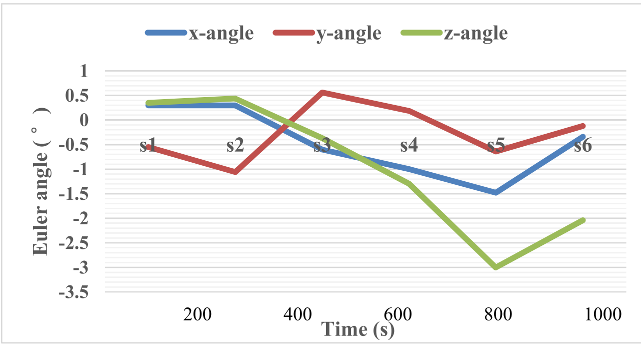

Fig. 8. Errors of the estimation results of the attitude of APP compared with the real attitude at seven different postures s1–s6.

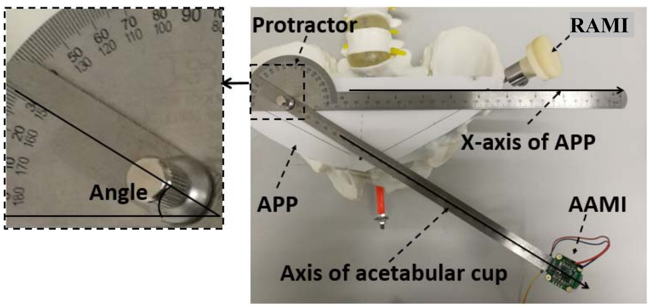

Fig. 9. Measurement system for implantation angles of acetabular cup; the real angle is measured by protractor.

axis represents the estimated Euler angle errors occurred in x-, y-, and z-angles. From Fig. 8, we find that the estimation errors of x- and y-angles are smaller than that of z-angle. The average estimation errors for x-, y-, and z-angles are $-0.47°$, $-0.27°$, and $-0.99°$ Euler angles, respectively.

Moreover, comparing the Euler angle of the real attitude and estimated attitude of APP in Table I, the root-mean-square errors (RMSEs) of x-, y-, and z-angles are 0.80°, 0.61°, and 1.57°, respectively. As the three-axis accelerometer in the IMU estimates the attitude by the gravity, it has less sensitivity in detecting rotations around z-axis. From the results in Fig. 8, we can also see that the RMSE of attitude estimation in z-axis is higher than that in x- and y-axes. According to [39] and [40], we obtain the standard uncertainties of attitude estimation around x-, y-, and z-axes, which are 0.11°, 0.09°, and 0.22°, respectively, and the overall expanded uncertainty of APP attitude estimation is 1.81° with a level of confidence of 95%.

C. Results of Implantation Angles of Acetabular Cup

In order to measure the implantation angles of acetabular cup during THR, we fix AAMI on one arm of protractor (shown in Fig. 9), and adjust the axis (represents the axis of acetabular cup) of the sensor module parallel to the arm, and the other arm of protractor aligned with the axis of pelvis, the real angles, used as a reference, between the axis of acetabular cup and pelvis can be read from the protractor directly. The estimated angles are calculated from the data collected by sensor modules, RAMI and AAMI.

The experimental results are shown in Fig. 10, from which we can see that the estimated angles agree with the real

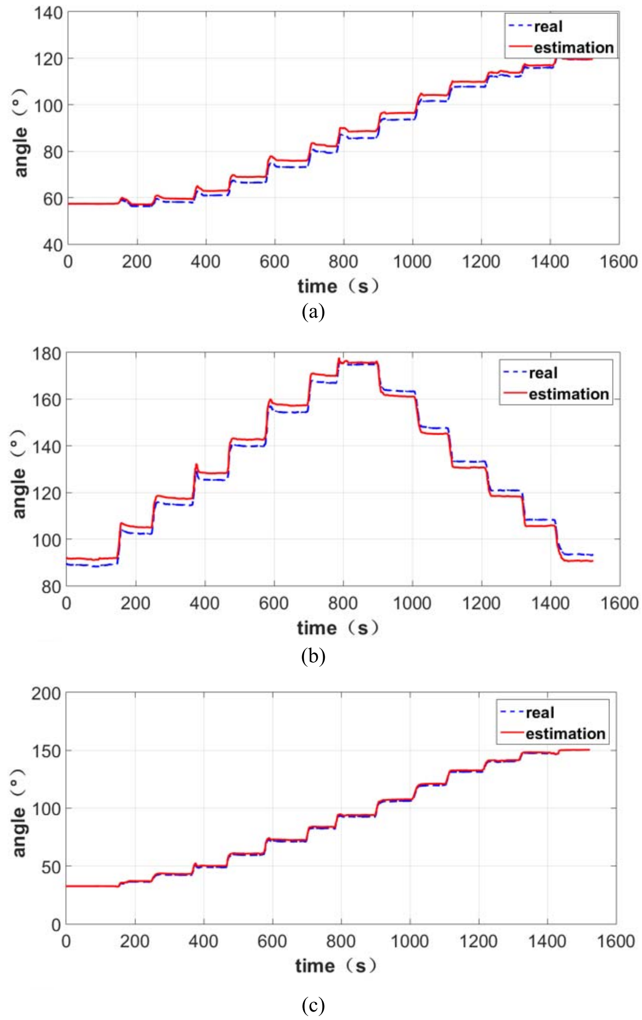

Fig. 10. Implantation angles of acetabular cup between (a) x-axis, (b) y-axis, and (c) z-axis of pelvis.

angles. The average error of estimated angles between x-, y-, and z-axes of acetabular cup and pelvis are 1.83°, 0.40°, and 0.99°, respectively, and their standard uncertainties are 0.14°, 0.37°, and 0.07°, respectively, according to [39] and [40]. The results show that the absolute error of acetabular cup attitude estimation is within 3°, which meets the requirement of the surgery. From Fig. 10, we also find that the estimation accuracies of the acetabular cup's implantation orientation according to x- and y-axes of the pelvis are worse than that according to z-axis. But these errors are more like a system error, which can be eliminated by calibration. The system error is mainly caused by the following aspects. First, surgeon's improper operation may bring errors. In other words, the IAMI instrument should be properly put on APP, that is, the three support feet of IAMI should be put on the three points ①, ②, and ③ (shown in Fig. 1). Second, the mismatch among the size of the instruments also contributes to the system error.

V. Conclusion

In this paper, an IMU-based system for attitude measurement of APP and implantation angles of prosthesis is proposed. The system is composed of three parts: IAMI, RAMI, and AAMI; IAMI is used to estimate the initial attitude of the APP, RAMI tracks the real-time attitude of the APP during the surgeries, and AAMI aims to obtain the implantation angles of the acetabular cup. The attitude data are acquired by multisensors, including an IMU and magnetometers, and is transmitted to PC through Bluetooth. A quaternion-based EKF is adopted as the data fusion algorithm to fuse the sensor data to attitude information. The attitude of the APP and implantation angles of acetabular cup are calculated through the algorithm designed in this paper. The experimental results show that the RMSE of attitude estimation of APP is less than 1.6°, with the standard uncertainty of less than 0.22°. The RMSE of implanting orientation estimation of acetabular cup is less than 3°, with an overall standard uncertainty of 0.17°. The accuracy of our system meets the requirement of the THR surgery and help surgeon make an accurate judgment of implants during the surgery, and as a result, the success rate the THR surgeries can be improved significantly. In the future work, the clinic experiments will be carried out.

VI. Acknowledgment

The authors would like to thank Dr. Y. Zhou and Dr. H. Tang from Jishuitan Hospital, Beijing, China, for their valuable suggestions and discussion with authors.

References

[1] S. Kurtz *et al.*, "Projections of primary and revision hip and knee arthroplasty in the United States from 2005 to 2030," *J. Bone Joint Surgery*, vol. 89, no. 4, pp. 780–785, 2007.

[2] D. Vashishth and D. Kim, "A hands-on approach to biomechanics education in total hip arthroplasty," in *Proc. 24th Annu. Conf. Annu. Fall Meeting Biomed. Eng. Soc. (EMBS/BMES)*, vol. 3. 2002, pp. 2615–2616.

[3] L. M. White *et al.*, "Complications of total hip arthroplasty: MR imaging—Initial experience," *Radiology*, vol. 215, no. 1, pp. 254–262, 2000.

[4] K. J. Saleh, R. Kassim, P. Yoon, and L. N. Vorlicky, "Complications of total hip arthroplasty," *Amer. J. Orthopedics*, vol. 31, no. 8, pp. 485–488, 2002.

[5] J. L. Nutt, K. Papanikolaou, and C. F. Kellett, "Complications of total hip arthroplasty," *Orthopaedics Trauma*, vol. 27, no. 5, pp. 272–276, 2003.

[6] M. Ghaffari, R. Nickmanesh, N. Tamannaee, and F. Farahmand, "The impingement-dislocation risk of total hip replacement: Effects of cup orientation and patient maneuvers," in *Proc. Int. Conf. IEEE Eng. Med. Biol. Soc.*, Aug. 2012, pp. 6801–6804.

[7] L. D. Dorr and Z. Wan, "Causes of and treatment protocol for instability of total hip replacement," *Clin. Orthopaedics Rel. Res.*, vol. 355, pp. 144–151, Oct. 1998.

[8] C. D. Fackler and R. Poss, "Dislocation in total hip arthroplasties," *Clin. Orthopaedics Rel. Res.*, vol. 151, pp. 169–178, Sep. 1980.

[9] L. Yuan and C. Shih, "Dislocation after total hip arthroplasty," *Arch. Orthopaedic Trauma Surgery*, vol. 119, nos. 5–6, pp. 263–266, 1999.

[10] J. Parvizi, E. Picinic, and P. F. Sharkey, "Revision total hip arthroplasty for instability: Surgical techniques and principles," *Instruct. Course Lectures*, vol. 58, no. 5, pp. 183–191, 2009.

[11] A. W. Blom, M. Rogers, A. H. Taylor, G. Pattison, S. Whitehouse, and G. C. Bannister, "Dislocation following total hip replacement: The Avon Orthopaedic Centre experience," *Ann. Roy. College Surgeons England*, vol. 90, no. 8, pp. 658–662, 2008.

[12] D. E. Mccollum and W. J. Gray, "Dislocation after total hip arthroplasty. Causes and prevention," *Clin. Orthopaedics Rel. Res.*, vol. 261, pp. 159–170, Dec. 1990.

[13] Z. Ren and W. Q. Yang, "Development of a navigation tool for revision total hip surgery based on electrical impedance tomography," *IEEE Trans. Instrum. Meas.*, vol. 65, no. 12, pp. 2748–2757, Dec. 2016.

[14] R. Biedermann, A. Tonin, M. Krismer, F. Rachbauer, G. Eibl, and B. Stöckl, "Reducing the risk of dislocation after total hip arthroplasty: The effect of orientation of the acetabular component," *J. Bone Joint J.*, vol. 87, no. 6, pp. 762–769, 2005.

[15] D. Kohn, O. Rühmann, and C. J. Wirth, "Dislocation of total hip endoprosthesis with special reference to various techniques," *Zeitschrift Orthopädie Und Ihre Grenzgebiete*, vol. 135, no. 1, pp. 40–44, 1997.

[16] G. E. Lewinnek, J. L. Lewis, R. Tarr, C. L. Compere, and J. R. Zimmerman, "Dislocations after total hip-replacement arthroplasties," *J. Bone Joint Surgery Amer.*, vol. 60, no. 2, pp. 217–220, 1978.

[17] L. D. Dorr, A. W. Wolf, R. Chandler, and J. P. Conaty, "Classification and treatment of dislocations of total hip arthroplasty," *Clin. Orthopaedics Rel. Res.*, vol. 173, pp. 151–158, Mar. 1983.

[18] B. C. Werner and T. E. Brown, "Instability after total hip arthroplasty," *World J. Orthopedics*, vol. 3, no. 8, pp. 122–130, 2012.

[19] D. W. Murray, "The definition and measurement of acetabular orientation," *J. Bone Joint J.*, vol. 75, no. 2, pp. 228–232, 1993.

[20] C. Nikou, B. Jaramaz, A. M. DiGioia, and T. J. Levison, "Description of anatomic coordinate systems and rationale for use in an image-guided total hip replacement system," in *Medical Image Computing and Computer-Assisted Intervention—MICCAI* (Lecture Notes in Computer Science), vol. 1935. Berlin, Germany: Springer-Verlag, 2000, pp. 1188–1194.

[21] G. Wu *et al.*, "ISB recommendation on definitions of joint coordinate system of various joints for the reporting of human joint motion—Part I: Ankle, hip, and spine," *J. Biomech.*, vol. 35, no. 4, pp. 543–548, 2002.

[22] W. Dandachli, R. Richards, V. Sauret, and J. P. Cobb, "The transverse pelvic plane: A new and practical referenceframe for hip arthroplasty," *Comput. Aided Surgery*, vol. 11, no. 6, pp. 322–326, 2006.

[23] K. H. Widmer, "Is there really a 'safe zone' for the placement of total hip components?" *Ceramics Orthopaedics*, vol. 75, no. 5, pp. 249–252, 2006.

[24] R. D. Lea and J. J. Gerhardt, "Range-of-motion measurements," *J. Bone Joint Surgery*, vol. 77, no. 12, pp. 784–798, 1995.

[25] I. Holm, B. Bolstad, T. Lütken, A. Ervik, M. Røkkum, and H. Steen, "Reliability of goniometric measurements and visual estimates of hip ROM in patients with osteoarthrosis," *Physiotherapy Res. Int.*, vol. 5, no. 4, pp. 241–248, 2000.

[26] S. Parratte, "Validation and usefulness of a computer-assisted cup-positioning system in total hip arthroplasty," *J. Bone Joint Surgery*, vol. 89, no. 3, pp. 494–499, 2007.

[27] S. Kobashi *et al.*, "MDCT image based assessment of acetabular cup orientation in total hip arthroplasty," in *Proc. IEEE Int. Conf. Syst., Man, Cybern. (SMC)*, Oct. 2014, pp. 2557–2562.

[28] A. M. DiGioia *et al.*, "Image guided navigation system to measure intraoperatively acetabular implant alignment," *Clin. Orthopaedics Rel. Res.*, vol. 355, pp. 8–22, Oct. 1998.

[29] J. Favre, R. Aissaoui, B. M. Jolles, J. A. de Guise, and K. Aminian, "Functional calibration procedure for 3D knee joint angle description using inertial sensors," *J. Biomech.*, vol. 42, no. 14, pp. 2330–2335, 2009.

[30] S. Šlajpah, R. Kamnik, and M. Munih, "Kinematics based sensory fusion for wearable motion assessment in human walking," *Comput. Methods Programs Biomed.*, vol. 116, no. 2, pp. 131–144, 2014.

[31] J.-X. Zhang, A. C. Novak, B. Brouwer, and Q. Li, "Concurrent validation of Xsens MVN measurement of lower limb joint angular kinematics," *Physiol. Meas.*, vol. 34, no. 8, pp. N63–N69, 2013.

[32] N. Enayati, E. D. Momi, and G. Ferrigno, "A quaternion-based unscented Kalman filter for robust optical/inertial motion tracking in computer-assisted surgery," *IEEE Trans. Instrum. Meas.*, vol. 64, no. 8, pp. 2291–2301, Aug. 2015.

[33] S. Sabatelli, M. Galgani, L. Fanucci, and A. Rocchi, "A double-stage Kalman filter for orientation tracking with an integrated processor in 9-D IMU," *IEEE Trans. Instrum. Meas.*, vol. 62, no. 3, pp. 590–598, Mar. 2015.

[34] P. Schopp, H. Graf, W. Burgard, and Y. Manoli, "Self-calibration of accelerometer arrays," *IEEE Trans. Instrum. Meas.*, vol. 65, no. 8, pp. 1913–1925, Sep. 2016.

[35] Z. Cao, S. Su, H. Chen, H. Tang, Y. Zhou, and Z. Wang, "Pose measurement of Anterior Pelvic Plane based on inertial measurement unit in total hip replacement surgeries," in *Proc. Int. Conf. IEEE Eng. Med. Biol. Soc.*, Aug. 2016, pp. 5801–5804.

[36] A. M. Sabatini, "Quaternion-based extended Kalman filter for determining orientation by inertial and magnetic sensing," *IEEE Trans. Biomed. Eng.*, vol. 53, no. 7, pp. 1346–1356, Jul. 2006.

[37] H. Zhao and Z. Wang, "Motion measurement using inertial sensors, ultrasonic sensors, and magnetometers with extended Kalman filter for data fusion," *IEEE Sensors J.*, vol. 12, no. 5, pp. 943–953, May 2012.

[38] T. Harada, H. Uchino, T. Mori, and T. Sato, "Portable orientation estimation device based on accelerometers, magnetometers and gyroscope sensors for sensor network," in *Proc. IEEE Int. Conf. Multisensor Fusion Integr. Intell. Syst. (MFI)*, Aug. 2003, pp. 191–196.

[39] JCGM, "Evaluating standard uncertainty," in *Proc. Eval. Meas. Data-Guide Expression Uncertainty Meas. (GUM)*, 2008, pp. 10–14.

[40] A. Ferrero and S. Salicone, "Measurement uncertainty," *IEEE Trans. Instrum. Meas.*, vol. 9, no. 3, pp. 44–51, Jun. 2006.

Hong Chen (S'03–M'07–SM'17) received the Ph.D. degree from the Department of Electronic Engineering, Tsinghua University, Beijing, China, in 2005.

From 2005 to 2007, she was a Post-Doctoral Fellow with the Institute of Microelectronics, Tsinghua University, where she is currently an Associate Professor. In 2006, she joined the Medical Center, Nebraska University, Lincoln, NE, USA, as a Visiting Scholar. In 2016, she joined the Department of Electronics and Computer Engineering, Georgia Tech, Atlanta, GA, USA, as a Visiting Scholar. She has authored 80 journal and conference papers and two books. She holds 18 granted Chinese and American patents. Her current research interests include monitoring-system design for total knee replacement/total hip replacement surgeries, low-power digital integrated-circuit designs, asynchronous circuit designs, PZT power electronics, and low-power mixed-signal SoC designs.

Dr. Chen was a recipient of the Best Demo Award at ISCAS 2013. She has been a Technologies Program Committee Member of ASYNC since 2014.

Zhe Cao received the B.S. degree from Yanshan University, Qinhuangdao, China, in 2014. He is currently pursuing the M.S. degree with the Department of Microelectronics and Nanoelectronics, Tsinghua University, Beijing, China.

His current research interests include system based on inertial sensors for pose measurement of anterior pelvic plane and implantation angles of prosthesis.

Shaojie Su received the B.S. degree from the School of Electronic Engineering, University of Posts and Telecommunications, Beijing, China, in 2012. He is currently pursuing the Ph.D. degree with the Department of Microelectronics and Nanoelectronics, Tsinghua University, Beijing.

His current research interests include visual aided system for total hip replacement surgeries.

Jie Liu is currently a Junior Student with the Microelectronics and Nanoelectronics Department, Tsinghua University, Beijing, China. Her current research interests include system based on inertial sensors for pose measurement of anterior pelvic plane and implantation angles of prosthesis.

Zhihua Wang (M'99–SM'04–F'17) received the B.S., M.S., and Ph.D. degrees in electronic engineering from Tsinghua University, Beijing, China. in 1983, 1985, and 1990, respectively.

He has been served as a Full Professor and the Deputy Director with the Institute of Microelectronics, Tsinghua University, since 1997 and 2000, respectively. From 1992 to 1993, he was a Visiting Scholar at CMU, Pittsburgh, PA, USA. From 1993 to 1994, He was with KU Leuven, Leuven, Belgium. From 2014 to 2015, he was a Visiting Professor at HKUST, Hong Kong. He has co-authored 11 books/chapters, over 146 (396) papers in international journals (conferences), and holds 97 Chinese and five U.S. patents. His current research interests include CMOS RFIC and biomedical applications, involving RFID, phase-locked loop, low-power wireless transceivers, and smart clinic equipment combined with leading edge RFIC and digital image processing techniques.

Dr. Wang has served as an AdCom Member of the IEEE SSCS from 2016 to 2019, a Technology Program Committee Member of the IEEE ISSCC from 2005 to 2011 and has been a Steering Committee Member of the IEEE A-SSCC since 2005. He has served as the Technical Program Chair for A-SSCC 2013, the Chairman for the IEEE SSCS Beijing Chapter from 1999 to 2009, a Guest Editor for the IEEE JOURNAL OF SOLID-STATE CIRCUITS Special Issues in 2006, 2009, and 2014, respectively, an Associate Editor of the IEEE TRANSACTIONS ON CIRCUITS AND SYSTEMS I, II and the IEEE TRANSACTIONS ON BIOMEDICAL CIRCUITS AND SYSTEMS, and other administrative/expert committee positions in China's national science and technology projects.